Propagation of Forecast Errors from the Sun to LEO Trajectories: How Does Drag Uncertainty Affect Conjunction Frequency?

John Emmert, Jeff Byers, Harry Warren, and Alan Segerman
Naval Research Laboratory

ABSTRACT

Atmospheric drag is the largest source of error in the prediction of trajectories of most objects in low-Earth orbit, and solar variability is the largest source of error in upper atmospheric density forecasts. There is thus a need to accurately propagate solar forecast uncertainty to atmospheric density uncertainty and thence to satellite position uncertainty. Furthermore, the collective position uncertainty of the low-Earth Orbit (LEO) population determines the frequency of conjunctions that must be assessed in order to avoid collisions. To maintain Space Situational Awareness of the growing LEO population, the number of conjunctions must be kept at a manageable level to avoid being overwhelmed by false alarms. This criterion can be used to define solar and atmospheric forecast accuracy requirements.

In this paper, we examine how solar forecast errors grow with increasing forecast time, and how this uncertainty maps to atmospheric density uncertainty as a function of altitude. We then develop analytical approximations of the mapping from density uncertainty to in-track position uncertainty, as a function of perigee height, orbital eccentricity, ballistic coefficient, background atmospheric conditions, and forecast time. Finally, we estimate the conjunction frequency between operational LEO satellites and the entire LEO population (separately considering objects larger than 10 cm and objects larger than 1 cm), based on the statistical distributions of the key orbital parameters (perigee height, eccentricity, inclination and ballistic coefficient) and assumed solar and density forecast uncertainties.

1. INTRODUCTION

Atmospheric drag is the largest source of uncertainty in the prediction of trajectories of most objects in low-Earth orbit [1]. The drag force is proportional to atmospheric density, and atmospheric density is in turn strongly controlled by incident ultraviolet radiation from the sun. Accordingly, modeling and forecasting upper atmospheric density and solar irradiance has been an active topic of research since the beginning of the space age. A fundamental issue in the application of this research to astrodynamics is the atmospheric accuracy needed to achieve a desired orbit prediction accuracy. The DoD's current density accuracy requirements [2] are ±5% below 500 km altitude, ±10% between 500 and 700 km, and ±15% above 700 km. These requirements are based on an Air Force Space Command (AFSPC) study. In a 2011 study, AFSPC proposed updated accuracy requirements to address more stringent orbit prediction requirements given in the Initial Capabilities Document for National Space Situational Awareness. The proposed requirements range from ±0.03% at low altitudes to ±61% at high altitudes.

A limitation of these requirements is that they are driven by position accuracy requirements that are the same for all objects, and which are motivated primarily by tactical awareness of operational payloads, rather than collision avoidance. In reality, how accurately one needs to know the position of a small piece of inert debris may be very different from the position accuracy requirements of an operational satellite. The distinction is very important in defining density accuracy requirements, because the atmospheric drag force (and its uncertainty) is inversely proportional to an object's size, which varies by several orders of magnitude in the current catalog.

To specifically address the collision avoidance problem, we studied the sensitivity of orbit prediction errors to solar irradiance and atmospheric density errors and how the position uncertainty grows with time as a forecast is extended further into the future. We then used this information to estimate how accurate density forecasts have to be to produce a specified frequency of collision alerts (defined as an operational satellite's position error overlapping with another object's position error).

In sections 2 and 3 below, we examine solar forecast uncertainties and atmospheric density uncertainties, respectively. In section 4, we quantify how these errors propagate to trajectory uncertainty. In section 5, we analyze

the distribution of in-track uncertainties for the catalogued LEO population, and derive the consequent frequency of conjunctions. Section 6 summarizes our results.

2. SOLAR FORECAST UNCERTAINTY

Solar extreme ultraviolet (EUV; wavelength 10–120 nm) radiation is the primary (but not the only) heating source of Earth's thermosphere and exosphere (altitudes above 120 km), and is the dominant driver of atmospheric density variations at these altitudes. The typical factor of two increase in EUV irradiance between solar minimum and solar maximum causes a factor of two increase in temperature and, at 400 km altitude, a factor of ten increase in density. Operational forecasts of EUV use statistical autoregressive models; an example of such a model is shown in Fig. 1.

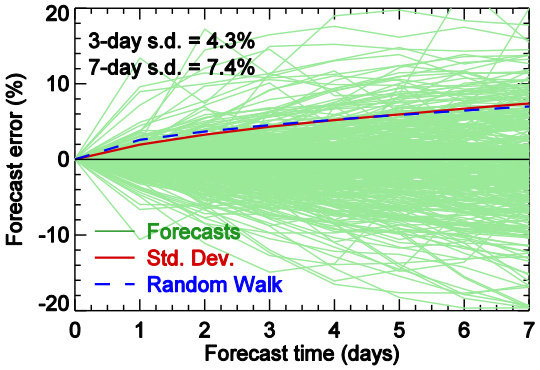

Fig. 1. Error of autoregressive (AR) forecasts of the S10 EUV index made during 2001. The forecasts were computed retrospectively using an AR(108) model trained on a random sampling of 1999–2013 data. Shown are forecast errors relative to the issued index (green), the standard deviation of the forecast errors (red), and the corresponding error growth of a random walk process (blue dashed).

The root-mean-square error grows approximately as the square root of the forecast time, and so it can be represented as a random walk process. The process is characterized by a single parameter: the root-variance at a given forecast time, which we denote σ_S. For this study, we initially use $\sigma_S = 7\%$ at a forecast time of 7 days, and we generate synthetic forecasts with hourly cadence. The top panel of Fig. 2 shows a 100-member ensemble of these forecast errors.

3. ATMOSPHERIC DENSITY FORECAST UNCERTAINTY

Density is highly sensitive to the temperature of the atmosphere: A hotter atmosphere is more extended, so density at a given altitude increases with increasing temperature. At LEO altitudes, temperature is approximately constant with height (with a value known as the exospheric temperature; in contrast, density decreases exponentially with increasing altitude). Exospheric temperature depends approximately linearly on EUV irradiance, so the error mapping is straightforward. Using the NRLMSISE-00® model [3], we obtain the following relationship:

$$\varepsilon_{T_{ex}} \cong (1.7 \text{ K/sfu})\varepsilon_S \qquad (1)$$

where $\varepsilon_{T_{ex}}$ is the exospheric temperature error in K and ε_S is the solar irradiance error in solar flux unit (sfu). The relative density error ($\varepsilon_\rho = \delta\rho/\rho$) associated with the temperature error is more complicated, and depends strongly on altitude and on the phase of the solar cycle. By differentiating the NRLMSISE-00® vertical density profile with respect to exospheric temperature and retaining on the dominant term, we obtain:

$$\varepsilon_\rho \cong \frac{\varepsilon_{T_{ex}}}{T_{ex}} \frac{gM_\rho}{kT_{ex}} \zeta \tag{2}$$

$g = 9.45$ m/s^2 = Gravity at 120 km

$M_\rho(z)$ = Mass-weighted mean molecular mass

$\zeta(z) = (z-120)(R_\oplus + 120)/(R_\oplus + z)$ = Geopotential height above 120 km

z = Geometric height above ground

The relative density error thus increases with height, but also decreases with decreasing molecular mass (which decreases with height). The net relative density error as a function of height, for a relative exospheric temperature error of 1%, is shown in Figure 3. The amplification factor is 2–3 near 200 km, maximizes at 8 in the region where atomic oxygen dominates and ranges from 3 to 5 above 1000 km, where helium is the dominant species.

Equations (1) and (2) are useful rules of thumb for estimating the density error, but computation of $M_\rho(z)$ in equation (2) still requires exercising a model like NRLMSISE-00®, so it is perhaps more straightforward, and potentially more accurate, to use the empirical model to propagate the errors directly. In the following sections, we take the latter approach.

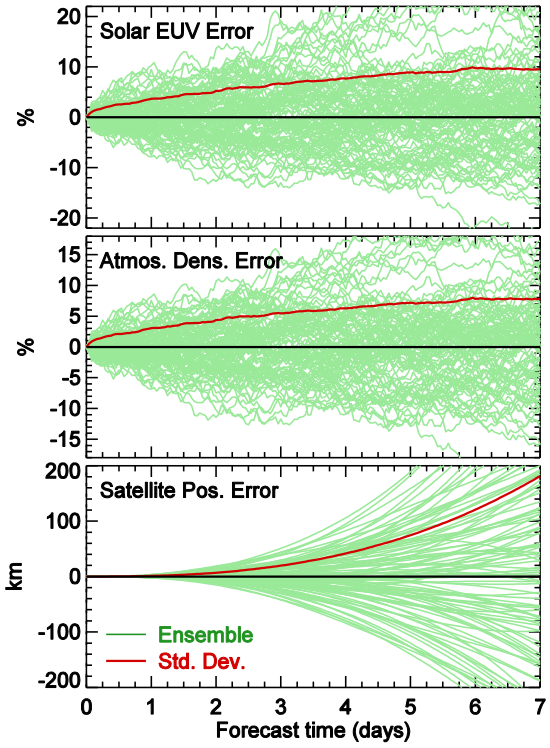

Fig. 2. (Top) Simulated 100-member, random-walk ensemble of EUV forecast errors, relative to a constant baseline of 130 solar flux units (sfu). The ensemble was constructed so that the root-variance is 7% at 7 days, with hourly cadence. Shown are the ensemble members (green) and their standard deviation (red). (Middle) The consequent relative density error at an altitude of 400 km, computed using the NRLMSISE-00® atmospheric model. (Bottom) The consequent in-track position error of a satellite in a 400 km circular orbit, with an inverse ballistic coefficient of $B = 0.1$ m^2/kg.

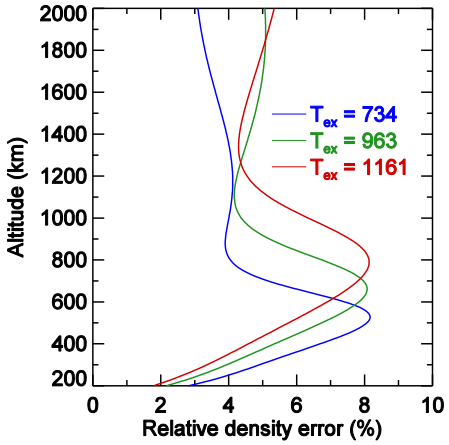

Fig. 3. Relative density error caused by a 1% error in exospheric temperature, under low (blue), moderate (green), and high (red) solar activity conditions.

4. ORBIT PREDICTION IN-TRACK UNCERTAINTY

Orbital drag causes a secular change in the orbital mean motion according to [4,5]:

$$\frac{dn}{dt} \cong \tfrac{3}{2} n^{1/3} \mu^{-2/3} \rho B v^3 \tag{3}$$

$n =$ Mean Motion

$\mu = GM_{\oplus}$

$B =$ Inverse ballistic coefficient

$v =$ Orbital speed

Thus, the error in the mean motion is related to the integral of the density error. The in-track position error is directly related to the mean anomaly M, which is related to the mean motion by

$$\frac{dM}{dt} = n \tag{4}$$

If density is underestimated, one finds the object farther along in its orbit than expected (or, conversely, one sees the object transit earlier than expected). This in-track position error is much larger than the drag-induced errors transverse to the orbital direction, which we neglect in this analyses. As indicated by equations 3 and 4, the effect is doubly compounded with time, because 1) drag continually increases the mean motion and 2) even if the mean motion error were fixed, the in-track error would progressively increase with each orbit. We found that the in-track error is approximately:

$$\varepsilon_{\|}(t) \cong \frac{v}{n}\left(\varepsilon_{M_0} + \varepsilon_{n_0} t + \frac{3}{2}\mu\rho_p B g(e,H) \frac{\sqrt{1-e}}{r_p^2} \int_0^t \int_0^{t'} \varepsilon_\rho(t'')\, dt''dt' \right) \quad (5)$$

ε_{M_0} = Error in the initial mean anomaly

ε_{n_0} = Error in the initial mean motion

t = Time

ρ_p = Atmospheric density at perigee

$g(e,H)$ = Adjustment factor for non-circular orbits

e = Eccentricity of orbit

H = Atmospheric density scale height

r_p = Perigee distance from Earth center

In this approximation, there are three terms that contribute to the in-track position error. The first term is due to the error in the mean anomaly (the orbital phase), and is directly related to the horizontal resolution of the tracking measurement. The second term is due to the error in the derived mean motion (or, equivalently, the semi-major axis orbital element); this term increases linearly with time. The third and most complex term is due to relative error in atmospheric density. This term also depends on time, being proportional to the cumulative double integral of the relative density error. It is also proportional to the density at perigee, to the object's ballistic coefficient (which in turn is proportional to the area-to-mass ratio), and to a factor g that accounts for the fraction of the orbit during which the object experiences significant drag. This factor is one for circular orbits, decreases as the eccentricity increases (object spends less time near the denser perigee), and decreases as the atmospheric scale height decreases (the atmosphere is more concentrated toward perigee. This factor is essentially the integrated drag around one orbit, relative to the drag at perigee. We numerically computed g as a function of eccentricity and scale height, and we developed the empirical approximation shown in Fig. 4. This function effectively summarizes (approximately) the more detailed expansions developed by King-Hele [4].

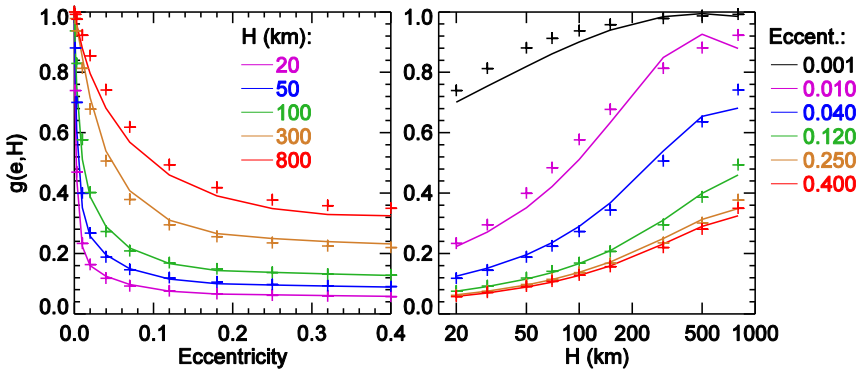

Fig. 4. Numerically computed $g(e,H)$ (symbols), and empirical approximation (solid lines). Results are shown as a function of orbital eccentricity e (left) and the log of the atmospheric scale height H (right).

The density scale height in the thermosphere increases with increasing temperature (which causes the thermosphere to expand and become more extended) and with decreasing mass of the dominant atmospheric species. Temperature is approximately constant with respect to height in the LEO regime, but the thermospheric composition is stratified, with the heavier molecules O_2 and N_2 dominating at the bottom, O dominating in the middle, and He and H at the top. The scale height thus increases monotonically with height from a few tens of kilometers around 400 km altitude to hundreds of kilometers above 1000 km altitude; it can be estimated from empirical atmospheric models.

Applying the relative density error process model of equation (3) to equation (5), we obtained the following approximation of how the variance of the in-track error grows with time, if the relative density error at perigee follows a random walk process:

$$\operatorname{var}\varepsilon_{\|}(t) \cong \left(\frac{v}{n}\right)^2 \left[\operatorname{var}\varepsilon_{M_0} + t^2 \operatorname{var}\varepsilon_{n_0} + \left(\frac{3}{2}\mu\rho_p Bg(e,H)\frac{\sqrt{1-e}}{r_p^2} \right)^2 \frac{t^5}{20}\frac{1}{\Delta t}\sigma_{\rho_0}^2 \right] \tag{6}$$

where Δt is the time step used to discretize the density error process and $\sigma_{\rho_0}^2$ is the variance of the relative density error ε_ρ at perigee at the first time step.

For a random walk density error process, the in track squared-error growth rate due to drag is faster (5th power of t) than the growth rate (t^2) due to errors in the initial mean motion. The drag-induced error will therefore eventually become larger than the orbital element errors. This happens more quickly for larger perigee density (i.e., lower perigee), larger ballistic coefficient (i.e., smaller objects), and more circular orbits. This helps explain why drag uncertainty is such a challenging problem for forecasting the trajectories of most of the LEO population.

Note that equation (5) neglects uncertainty in the ballistic coefficient, and focuses instead on the trajectory error attributable to atmospheric density uncertainty. Errors in B could be incorporated into equation (5); we expect that their variances are typically more temporally uniform than those of the density forecast errors, so that the consequent in-track error variance growth rate would be slower (3rd power of t instead of the 5th power).

We have validated the third term in equation (6) by generating ensembles of trajectories with an orbit propagator, assuming perfect knowledge of the orbit at $t = 0$. An example is shown in the bottom panel of Fig. 1.

5. CONJUNCTION FREQUENCY DUE TO ATMOSPHERIC DENSITY UNCERTAINTY

We used equation (6) (with the initial mean motion and mean anomaly uncertainties set to zero) to estimate the conjunction frequency between operational satellites and orbital debris in the current TLE catalog.

We seeded the density uncertainty with a random walk process for the EUV forecast, as shown in the top panel of Fig. 1. We discretized the process with a time step of 1 hour; for our initial computation, we used a solar EUV irradiance uncertainty of 7% at a forecast time of 7 days, so that the forecast error at the first time step (t = 1 hour) is 0.52%. We then used NRLMSISE-00® to compute the values of $\sigma_{\rho_0}^2$, ρ_p, and H in equation (6) for each object. For the ballistic coefficients B, we used values estimated as described in [6]; these only cover a portion of the catalog, so we applied their statistical distribution to obtain simulated values for the remaining objects. Fig. 5 shows the distribution of in-track uncertainty as a function of perigee altitude, for a background solar activity level of $F_{10.7}$ = 130 sfu, which corresponds to moderate solar activity.

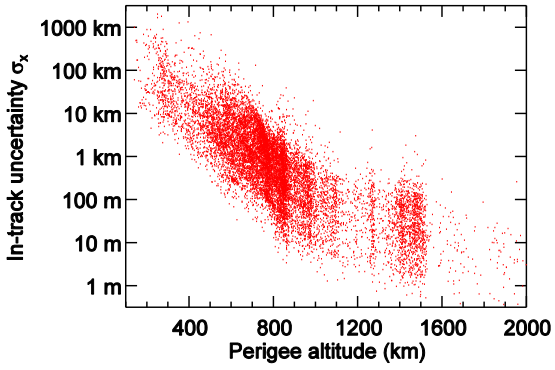

Fig. 5. In-track uncertainty of the LEO catalog due to atmospheric density uncertainty, as a function of perigee altitude. The results shown correspond to a forecast time of 7 days with EUV irradiance uncertainty of 7%.

The drag-induced in-track uncertainties are accompanied by much smaller but perfectly correlated cross-track (primarily radial) uncertainties. In order to define an uncertainty volume for conjunction analysis, we need to specify an independent cross-track uncertainty; we arbitrarily chose a constant value of 100 m (in reality, the cross track uncertainty will depend on the object). We then define the uncertainty volume as a curved cylinder along the nominal orbital track, with radius 100 m and a length of +/- the 1-sigma in-track uncertainty, as illustrated in Fig. 6.

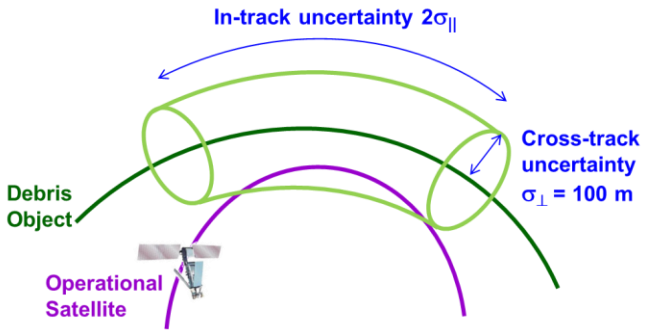

Fig. 6. Geometry used for conjunction analysis.

For the purpose of identifying conjunctions, we assumed unperturbed orbits. We computed the Keplerian orbital elements for each object based on the state vector at the TLE epoch. We then computed the minimum distance between each operational satellite (~500 objects) and each non-operational object (~13,000 objects), using the algorithm described in [7]. From the ~6 million pairs of objects, we selected pairs with minimum distances less than our cross-track threshold of 100 m, about 3,400 pairs. For each pair, we then identified all critical points with distances less than 100 m. Usually, only one critical point satisfies this criteria, but for some pairs there are multiple possible conjunctions. In this way, we identified ~3,900 possible conjunctions, defined by pairs of eccentric anomalies (and hence mean anomalies) for each pair of objects.

We assumed that the mean anomalies of the operational satellites have zero uncertainty (due to their typically much larger area-to-mass ratios, the effect of atmospheric drag is generally small compared to debris objects). Then, for each possible conjunction, the operational satellite attains the appropriate mean anomaly value with a frequency equal to the mean motion:

$$f_{MA_1} = n_1 \text{ (expressed as revolutions/time)} \tag{7}$$

At a random time, the probability that the uncertainty cylinder of the non-operational object encompasses its conjunction mean anomaly is proportional to its mean anomaly uncertainty (expressed in radians):

$$p_{MA_2} = \frac{\sigma_{MA_2}}{2\pi} \tag{8}$$

The frequency of each conjunction is thus

$$f_{conj} = f_{MA_1} p_{MA_2} \tag{9}$$

Fig. 7 shows the resulting total frequency of conjunctions as a function of conjunction altitude (equation (9) summed over object pairs in 50 km altitude bins) and background solar activity level (summed over all pairs).

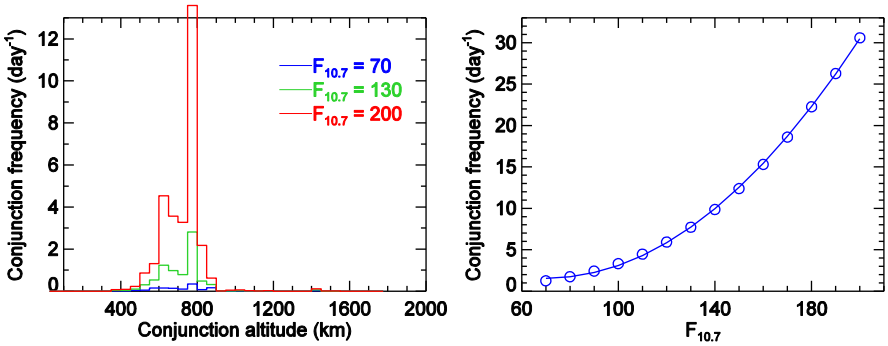

Fig. 7. Conjunction frequency between operational and non-operational objects, due to atmospheric density uncertainty. (Left) Conjunction frequency summed in 50 km bins of the conjunction altitude, for low (blue), moderate (green), and high (red) solar activity conditions. (Right) Total conjunction frequency as a function of solar activity (as represented by the $F_{10.7}$ index). The circles show the computed frequency, and the solid line is a quadratic fit to the circles. The results shown correspond to a forecast time of 7 days with EUV irradiance uncertainty of 7%, and a cross-track uncertainty of 100 m.

The conjunctions are heavily concentrated in the 400–900 km altitude region. At lower altitudes, the debris population is too sparse to produce frequent conjunctions; at higher altitudes, the atmosphere is too thin to generate appreciable in-track uncertainty. The conjunction frequency peaks in the 750–800 km bin, with a secondary peak near 600 km. The total conjunction frequency increases approximately quadratically with increasing background EUV irradiance; the altitude dependence largely retains its character from solar minimum to solar maximum.

Our test case of 7% EUV irradiance uncertainty after 7 days can be approximately extrapolated to other input parameters. Inspection of equations (6), (8), and (9) suggests (and we have empirically confirmed) that the conjunction frequency is directly proportional to the relative EUV uncertainty and to the 5/2 power of the forecast time. We have also found that the conjunction frequency is proportional to the assumed cross track uncertainty.

We also wish to extrapolate our results to the larger population of > 1 cm debris. Fig. 8 shows the density of orbiting objects as a function of altitude, for operational satellites and the current TLE catalog, as well the >1cm and >10 cm populations from NASA's ORDEM 2000 debris model. The distribution shows that the catalog is approximately the same as the >10 cm debris model. The >1 cm population is approximately ten times larger, a factor that is roughly the same for all LEO altitudes. The conjunction frequency should increase proportionally to the size of the population (the operational population against which conjunctions are evaluated is fixed). In addition, the distribution of B should be shifted toward larger values in the >1 cm population, due to its larger area-to-mass ratios. Since A/m is inversely proportional to the characteristic length of an object, we expect that consideration of the 1–10 cm population would lead to an additional factor of ten increase in the conjunction frequency, for an overall factor of 100.

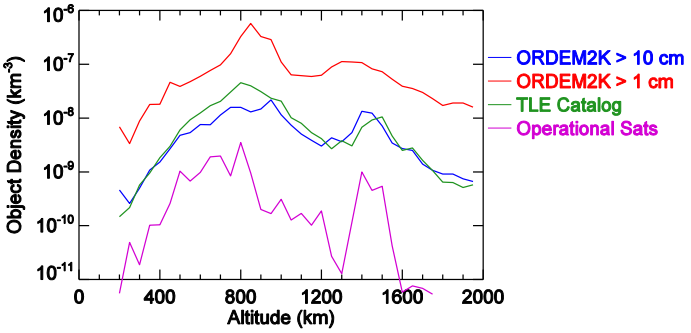

Fig. 8. Log-density of LEO objects in 2010 as a function of altitude, for operational satellites (purple), the TLE catalog (green), the >10 cm population of NASA's ORDEM 2000 debris model (blue), and the >1 cm population of ORDEM 2000 (red).

We can summarize the extensions discussed above into the following approximation:

$$f \cong f_0\left(F_{10.7}\right)\frac{N}{N_0}\frac{\langle B\rangle}{\langle B\rangle_0}\left(\frac{t}{t_0}\right)^{5/2}\left(\frac{t_0}{t}\right)^{1/2}\frac{\sigma_S}{\sigma_{S0}}\frac{\sigma_\perp}{\sigma_{\perp 0}}$$

$f =$ Total conjunction frequency	$f_0 = 1.24\ \mathrm{d}^{-1},\ \mathrm{F}_{10.7} = 70$ $f_0 = 7.71\ \mathrm{d}^{-1},\ \mathrm{F}_{10.7} = 130$ $30.6\ \mathrm{d}^{-1},\ \mathrm{F}_{10.7} = 200$
$N =$ No. of debris objects	$N_0 \cong 12,600$
$\langle B\rangle =$ Average inverse ballistic coefficient	$\langle B\rangle_0 \cong 0.25\ \mathrm{m}^2/\mathrm{kg}$
$t =$ Forecast time	$t_0 = 7$ days
$\sigma_S =$ EUV forecast uncertainty at time t_0	$\sigma_{S0} = 7.0\%$
$\sigma_\perp =$ Cross-track uncertainty	$\sigma_{\perp 0} = 100$ m

(10)

where the '0' subscripts denote the conditions used to produce Fig. 7. Note there are two adjustments involving the forecast time: one to adjust for in-track uncertainty growth rate (5/2 power), and one to adjust for the EUV uncertainty growth rate (1/2 power). From equation (10), we can estimate the EUV forecast uncertainty needed for a desired conjunction frequency:

$$\sigma_S \cong \sigma_{S0}\frac{f}{f_0\left(F_{10.7}\right)}\frac{N_0}{N}\frac{\langle B\rangle_0}{\langle B\rangle}\left(\frac{t_0}{t}\right)^2\frac{\sigma_{\perp 0}}{\sigma_\perp} \tag{11}$$

So, for example, if one desires a maximum of 5 conjunctions per day at a forecast time of 3 days, then for $F_{10.7}$ = 130, the EUV forecast uncertainty (at t = 3 days) must be less than ~25% for the current catalog:

$$(7\%)\cdot\left(\frac{5\ \mathrm{day}^{-1}}{7.71\ \mathrm{day}^{-1}}\right)\cdot 1\cdot 1\cdot\left(\frac{7\ \mathrm{day}}{3\ \mathrm{day}}\right)^2\cdot 1 = 25\% \tag{12}$$

For the >1 cm population, as discussed above, this criterion would be reduced by a factor of ~100, to 0.25%.

6. SUMMARY

We developed approximate expressions for the propagation of solar irradiance forecast errors propagate to atmospheric density forecasts to in-track orbit prediction errors. Root-mean-square solar forecast errors grow approximately as the square root of time during 7-day forecasts; thus, the errors are similar to a random walk process. The consequent density errors also grow at the same rate, but the resulting in-track position errors grow as the 5/2 power of time, due to their dependence on the double integral of the density error.

Applying these growth rates to the catalogued LEO population with selected ancillary parameters (cross-track uncertainty, solar cycle phase, solar forecast error magnitude), we estimated the frequency of conjunctions, attributable to atmospheric density uncertainty, between operational satellites and debris. For 7-day forecasts, the estimated conjunction frequency is 8 per day, occurring mostly in the 400–900 altitude range and peaking near 800 km. We also find that the conjunction frequency with the >1 cm debris population would be about a hundred times greater, due to the larger size of the population and its smaller area-to-mass ratios.

ACKNOWLEDGEMENTS

This work was supported by the Office of the Assistant Secretary of Defense for R&E, via the Data-to-Decisions program, and by the Office of Naval Research.

REFERENCES

1. Storz, M. F., B. R. Bowman, M. J. I. Branson, S. J. Casali, and W. K. Tobiska, High accuracy satellite drag model (HASDM), *Adv. Space Res., 36*, 2497–2505, 2005.
2. U.S. Space Command/J3 (1988), "Requirements for Improved Density Models" Memo, 18 April 1988.
3. Picone, J. M., A. E. Hedin, D. P. Drob, and A. C. Aikin, NRLMSISE-00 empirical model of the atmosphere: Statistical comparisons and scientific issues, *J. Geophys Res., 107*, doi:10.1029/2002JA009430, 2002.
4. King-Hele, D., *Satellite Orbits in an Atmosphere: Theory and Applications*, Blackie and Son Ltd., Glasgow, 1987.
5. Picone, J. M., J. T. Emmert, and J. L. Lean, Thermospheric densities derived from spacecraft orbits: Accurate processing of two-line element sets, *J. Geophys Res., 110*, A03301, doi:10.1029/2004JA010585, 2005.
6. Emmert, J. T., A long-term data set of globally averaged thermospheric total mass density, *J. Geophys Res., 114*, A06315, doi:10.1029/2009JA014102, 2009.
7. Baluyev, R. V., and K. V. Kholshevnikov, Distance Between Two Arbitrary Unperturbed Orbits, *Celestial Mechanics and Dynamical Astronomy, 93*, 287–300, 2005.